Experimental and computational studies of an antiplasmodial derivative of allantoin; antimycobacterial essential oil from *Cordia batesii* WERNHAM (Boraginaceae)

Eric Robert Tiam[1], Dominique Serge Ngono Bikobo[1], Ibrahim Mbouombouo Ndassa[2,3], Norbert Mbabi Nyemeck II[1], Auguste Abouem A Zintchem[1,3*], Lawrence Ayong[4], Patrick Hervé Betote Diboué[5], Bruno Lenta Ndjakou[1,3], Joséphine Ngo Mbing[1†] and Dieudonné Emmanuel Pegnyemb[1†]

Abstract

Background: Chemical and pharmacological investigations were performed on the stems of *Cordia batesii* (Boraginaeae); chemical studies included quantum calculations applied on a newly described compound.

Results: A new derivative of allantoin (**1**) named batesiin (**2**) was characterized. Thirteen other known compounds involving allantoin (**1**) were either isolated or identified. GC–MS enabled the identification of six compounds from a fraction containing essential oil. MeOH extract and some isolated compounds were tested in vitro against *Pf*7G8 CQS and *Pf* Dd2 CQR strains of *Plasmodium falciparum*; extract disclosed a moderate antiplasmodial activity ($IC_{50} = 50$ µg mL^{-1}). Meantime, the CH_2Cl_2 extract and essential oil fraction were tested on a resistant mycobacterial strain of *Mycobacterium tuberculosis*; a potent antimycobacterial activity with a MIC $= 9.52$ µg mL^{-1} was deduced from essential oil. Density functional theory (DFT) calculations were carried on batesiin (**2**). Calculated chemical shifts at B3LYP/6-31G(d,p) and MPW1PW91/6-31G+(d,p) showed much better correlations with the experimental data. Time dependent DFT at B3LYP/6-31G+(d,p) displayed a major absorption band 3.01 nm higher than the experimental value.

Conclusion: *Cordia batesii* can be considered as promising in search of compounds with antimalarial and antitubercular properties. DFT studies are very helpful when trying to learn more about the spectroscopic insights of a derivative of allantoin (**1**).

Keywords: *Cordia batesii*, Allantoin, Batesiin, Spectroscopy, Essential oil, DFT, Molecular orbitals, *Plasmodium falciparum*, *Mycobacterium tuberculosis*

Introduction

One of the main goals of World Health Organization (WHO) is to end the epidemics of neglected tropical diseases, tuberculosis (TB) and malaria (which remains the major public health and mortality problem in the tropics) by 2030 [1, 2]. In 2018, TB infected about 10.0 million people, mainly in WHO regions of South-East Asia (44%), Africa (24%) and the Western Pacific (18%); in parallel, about 213 million cases of malaria were found

*Correspondence: augabouem@yahoo.fr
†Joséphine Ngo Mbing and Dieudonné Emmanuel Pegnyemb contributed equally to this work
[1] Department of Organic Chemistry, Faculty of Science, University of Yaoundé I, P.O Box 812, Yaounde, Cameroon
Full list of author information is available at the end of the article

Tiam *et al. BMC Chemistry*   (2021) 15:15

Page 2 of 17

in the WHO African region. In the same year, half a million newly rifampicin-resistant TB cases were estimated. In general, 3.4% of new TB cases and 18% of formerly cured patients displayed either multidrug resistant TB or rifampicin-resistant TB (MDR/RR-TB) [3–5]. Trying to overcome the high cost or the shortage of drugs for treatment of malaria remains a challenge for chemists, and some authors proposed the synthesis of compounds disclosing an imidazole unit with efficient activities against malaria [6]. Recently, Al-Otaibi et al. [7] reported quantum calculations achieved on such derivatives; in their work, the authors evaluated the structural and electronic traits of those derivatives. ^{1}H- and ^{13}C-NMR spectroscopy is a central tool in the structure elucidation of organic compounds. A review by Lodewyk et al. [8] emphasized on computational predictions of NMR data on synthetic organic compounds and natural products. Natural products can be isolated from plants, which are considered to be an important source of major compounds in drug development because of their successful use in treating various human ailments since millenniums. In this context, searching for new natural products from medicinal plants could provide new ways for antimalarial and antitubercular drugs. Among these plants, some species of the genus *Cordia* (Boraginaceae) are reported to be useful in the treatment of tuberculosis, bronchitis and malaria [9].

The genus *Cordia* (Boraginaceae) is composed of trees or shrubs and is widespread in Central and South America, India, Asia and Africa [10]. Previous phytochemical investigations of plants from this genus reported the isolation and characterization of different classes of secondary metabolites including naphthoquinones, hydroquinones [11] or polyphenols [12]. Concurrently and based on some pharmacological surveys, essential oils from *C. curassivica* and *C. gilletii* appeared as active against some microbial strains [13, 14]. Biological activities and in silico investigations of *C. dichotoma* were recently reported [15]; the plant is also known to contain, apart from allantoin (**1**) [16, 17] which has been the subject of many quantum calculations [18, 19], fatty acids (FA) [20]. FA have been recognized as energy sources for *M. tuberculosis* inside host tissues and are supposed to induce dormancy in *Mycobacterium* bacilli [21, 22]. A few *Mycobacterium* bacilli were inhibited by *C. sebestena* extracts as results of biological analyses [23]. Sebestenoid D is a component of the latter species and was a matter of density functional theory (DFT) studies, with its optimized molecular geometry and HOMO–LUMO plot as outcomes [24, 25]. Highest occupied molecular orbital (HOMO) and lowest unoccupied molecular orbital (LUMO) were also calculated during a survey aiming to check the coherence between experimental and

theoretical NMR and IR data; this investigation was done on a compound with an imidazole unit [26] like allantoin (**1**). Other simulations completed on a particular range of complex natural products involved IR as well as electronic transitions for UV analyses through time dependent DFT (TD-DFT); findings were afterwards compared to experimental results [27].

Despite the intensive work performed on some *Cordia* species, no or less investigation has been done on *Cordia batesii* species, maybe because of its limited geographic location. In our continuing search of secondary metabolites with powerful antiplasmodial and antitubercular activities, chemical investigations were carried on the stems of *Cordia batesii*, a forest shrub growing in the central and western regions of Cameroon. This paper describes the isolation of a new derivative of **1** named batesiin (**2**) along with other compounds. In vitro activities regarding extracts of stems and some isolated compounds against two CQR strains of *Plasmodium falciparum* were examined, when essential oil from the plant was tested against a resistant mycobacterial strain of *Mycobacterium tuberculosis*. The detailed characterization of **2** was investigated based on experimental NMR and UV–visible spectroscopic analyses; DFT at B3LYP/6-31G(d,p) [28, 29] and MPW1PW91/6-31G+(d,p) [30, 31] and TD-DFT simulations at B3LYP/6-31G+(d,p) were then undertaken on the alleged structure. These quantum calculations were applied on **2** for two main reasons: the compound is described for the first time, its NMR data are closed to chemical shifts of **1** but the UV–visible spectra of both seem different. DFT calculations at B3LYP/6-311G++(d,p) were also performed to check some electronic and thermodynamic properties of **2**.

Results
Experimental results
Compounds **1**, **3**–**14** were identified based on comparison of their physical and spectral data with authentic samples or those already reported (Fig. 1). Their assignments were consistent with structures of: allantoin (**1**) [32], pyrimidine 2,4-(1*H*,3*H*)-dione (**3**) [33], cordialin A (**4**) and cordialin B (**5**) [34], quercetin (**6**) [35], myricetin (**7**) [36], genistein 4′-*O*-glucuronide (**8**) [37], methyl palmitate (**9**) [38], palmitic acid (**10**) [39], methyl (9*E*,12*E*)-octadeca-9,12-dienoate (**11**) [40], methyl oleate (**12**) [41], methyl tridecanoate (**13**) [42] and (*Z*)-octadec-11-enoic acid (**14**) [43].

Characterization of compound 2
Compound **2** was isolated as a white solid from CH_2Cl_2/MeOH mixture. Its molecular formula was deduced as $C_7H_8N_6O_5$ from the ESI-MS signal at *m/z* 257.4 $[M+H]^+$ and from the HR-LC/MS signal at *m/z* 279.1603

Tiam *et al. BMC Chemistry*   (2021) 15:15

Page 3 of 17
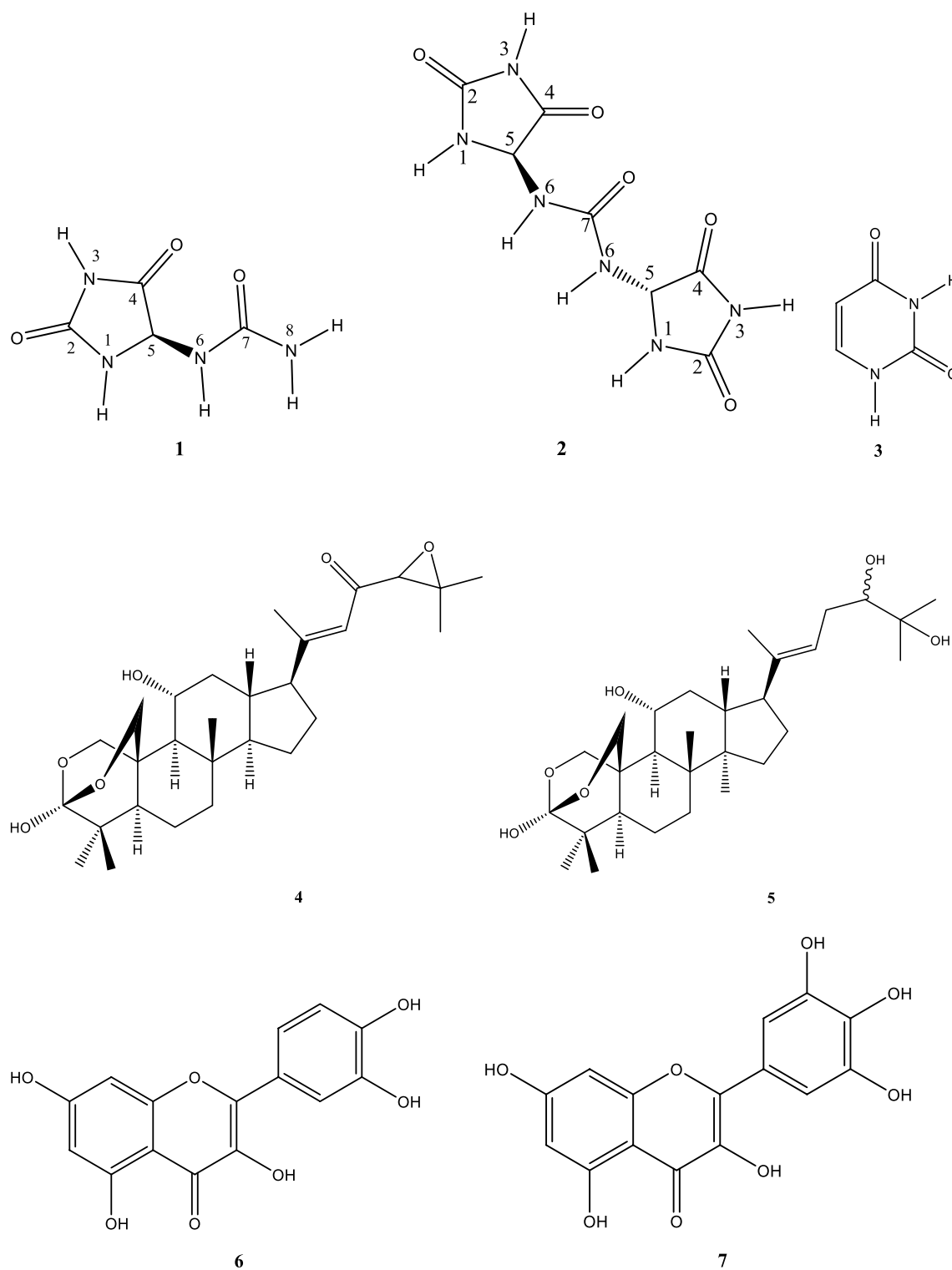
Fig. 1 Structures of the isolated/identified compounds (**1–14**) from the stems of *C. batesii*

Tiam *et al. BMC Chemistry*   (2021) 15:15

Page 4 of 17

8

9

10

11

12

13

14

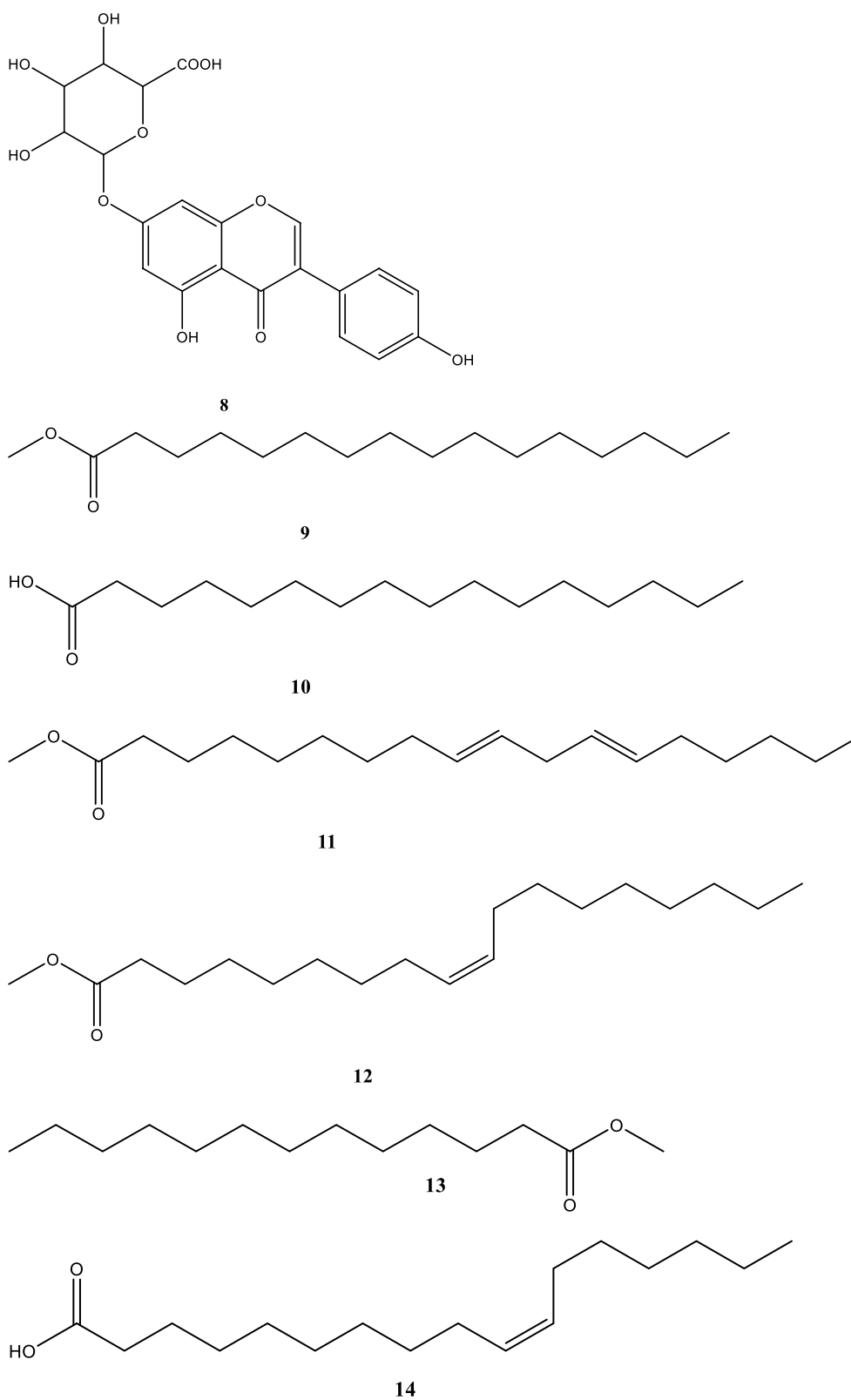**Fig. 1** continued

Tiam *et al. BMC Chemistry*   (2021) 15:15

Page 5 of 17

[M+Na]$^+$, in accordance with seven degrees of unsaturations. Additional data from the ESI-MS spectrum displayed other peaks at *m/z* 159.4 [M$_1$+H]$^+$ and 181.6 [M$_1$+Na]$^+$ which are characteristics of allantoin (**1**) [44]. These preliminary data suggested a close relationship between allantoin (**1**) and compound **2**. The ^{1}H-NMR spectrum of **2** exhibited a very prominent peak at δ$_H$ 5.30 (2H, d, ^{3} *J*(H,H) = 2.0 Hz, H–C(5)) ppm. Moreover, we observed from the same spectrum some signals attributable to protons attached to heteroatoms (especially to nitrogen) with chemical shifts at δ$_H$ 8.04 [2H, s, H–N(1)], 10.51 [2H, s, H–N(3)], 6.86 [2H, d, ^{3} *J*(H,H) = 2.0 Hz, H–N(6)] ppm (Table 1).

The ^{13}C-NMR spectrum of **2** showed four remarkable signals at 157.4 [C(2), 2C], 173.6 [C(4), 2C], 62.4 [C(5), 2C] and 156.8 [C(7), 1C] ppm; when considering that **2** contains seven carbon atoms, the number of

aforementioned signals presume the occurrence of a symmetry. The DEPT 135 NMR spectrum of **2** revealed one signal at δ$_C$ 62.4 [C(5)] ppm indicating one methine group. These observations were confirmed by its HSQC spectrum which indicates a correlation between the proton at δ$_H$ 5.30 ppm [H–C(5)] and the said carbon. Two remaining signals from the ^{13}C NMR spectrum are observable at δ$_C$ 48.6 and 54.9 ppm and are suggestive of signals of MeOH and CH$_2$Cl$_2$ respectively; this assertion is strengthened by correlations between signals at δ$_C$ 48.6 and δ$_H$ 3.17 ppm in one side, and signals at δ$_C$ 54.9 and δ$_H$ 5.74 ppm from the same HSQC spectrum [45].

The HMBC spectrum exhibited noticeable correlations between protons at δ$_H$ 5.30 ppm [H–C(5)] and the carbon atoms at δ$_C$ 173.6 ppm [C(4)] and 156.8 ppm [C(7)], between protons at δ$_H$ 6.88 ppm [H–N(6)] and carbon atoms at δ$_C$ 173.6 ppm [C(4)], 62.4 [C(5)] and 156.8 [C(7)]. Other correlations were found between nitrogenous protons at δ$_H$ 8.04 [H–N(1)] ppm and carbon atoms at δ$_C$ 157.3 ppm [C(2)], δ$_C$ 173.6 ppm [C(4)] and 62.4 ppm [C(5)]. The UV spectrum of **2** (Fig. 2) exhibited one major maximum at λ$_{max}$ = 296 nm, different from values of **1** [19].

Lakshmanan et al. [44] confirmed through an X-ray analysis that the occurring enantiomer of **1** is its (*S*) one. A thorough analysis of all the spectra and comparison with data from the literature revealed that compound **2** is described for the first time as a new derivative of allantoin (**1**); it was identified as (*S,S*)-1,3-bis(2,5-dioxoimidazolidin-4-yl)urea, trivially named batesiin (**2**). Table 1 shows some NMR data of allantoin (**1**) and batesiin (**2**); it strengthens the agreement of a close relationship

Table 1 ^{1}H- and ^{13}C-NMR 1D and 2D spectroscopic data of 1 and 2 (500 and 125 MHz in DMSO-*d$_6$*) in ppm

Position	Allantoin (1) [50, 61]		Batesiin (2)	
	δ$_C$	δ$_H$	δ$_C$	δ$_H$ (m, J)
2	156.7	–	156.8	–
4	173.4	–	173.6	–
5	62.3	5.23	62.4	5.30 (d, 2.0 Hz, 2H)
7	157.4	–	157.4	–
H–N(1)	–	8.04	–	8.04 (s, 2H)
H–N(3)	–	10.62	–	10.51 (s, 2H)
H–N(6)	–	6.88	–	6.88 (d, 2.0 Hz, 2H)
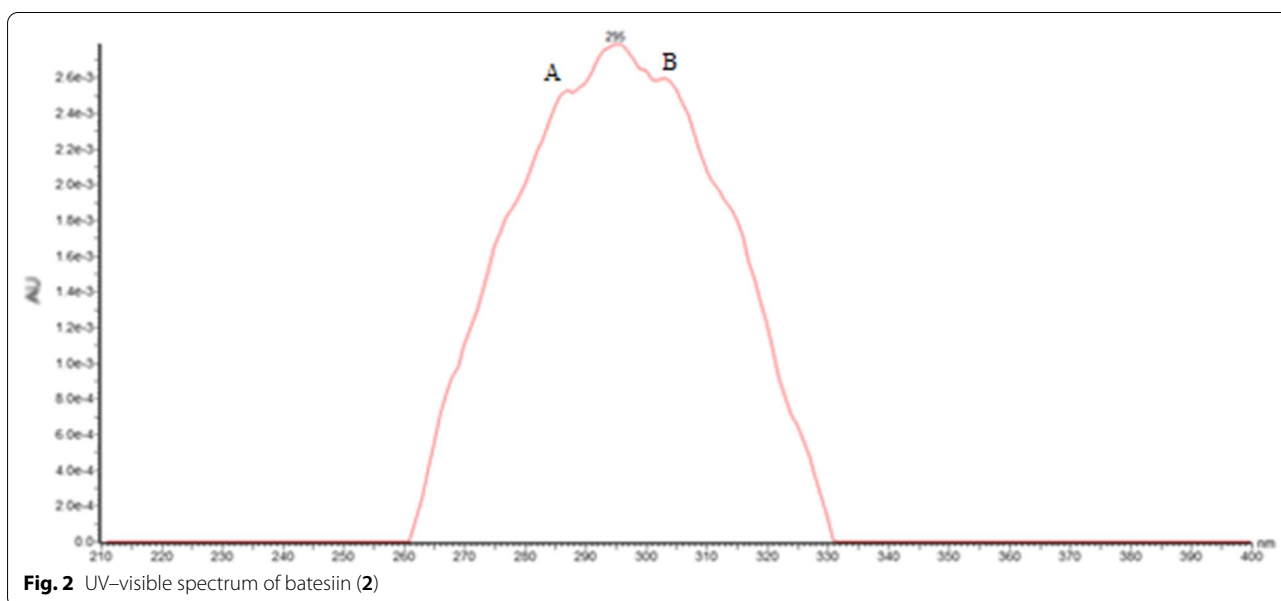
Fig. 2 UV–visible spectrum of batesiin (**2**)

Tiam *et al. BMC Chemistry*   (2021) 15:15

Page 6 of 17

between those two compounds in terms of NMR spectroscopic data.

Biological properties

The antimalarial efficiency of screening against *P. falciparum* Dd2 and 7G8 (CQR) strains of the MeOH extract of stems of *C. batesii* and compounds **2**, **3**, **5** and **6** was performed according to the Sybr Green I fluorescence-based assays [46]. The results are presented in Fig. 3; they indicate the IC_{50} of extract of stems of *C. batesii* and the percentage of growth inhibition against Dd2 and 7G8 *P. falciparum* strains respectively.

Figure 3a mentioned that the MeOH extract of stems discloses an $IC_{50} = 50$ µg mL^{-1} against Dd2 *P. falciparum* strain which can be considered as a moderate activity. It appears from Fig. 3b that, apart from artemisinin (95.75% of inhibition) used as reference, the MeOH extract has the highest antiplasmodial activity with 88.24% percentage inhibition followed by **2** with approximately 78% of growth inhibition against Dd2 strain. Compounds **3** and **5** showed high activity (>65%) of inhibition, exhibiting a growth inhibition of Dd2 strain *P. falciparum* with percentages corresponding to 66.43% and 72.99% respectively.

When tested against 7G8 *P. falciparum* strain, MeOH extract and compounds **2**, **3** and **5** displayed the percentages of growth inhibition of 18.82%, 34.26%, 10.04% and 2.84% at 10 µg mL^{-1} respectively. The same extract and isolated compounds at 100 µg mL^{-1} unveiled 25.03%, 63.86%, 98.07% and −18.44% of percentages of growth inhibition. These results are summarized in Fig. 3c and admit that **2** and **3** present the highest inhibition percentage (>60%) on 7G8 *P. falciparum* strains.

From the antimycobacterial tests results (Table 2), it should be noticed that the mixture of FA (A₁) exhibited a good antitubercular activity with a Minimal Inhibitory Concentration (MIC) value at 9.52 µg mL^{-1}. According to Cantrell et al. [47], isolated compounds that exhibit a MIC ≤ 64 µg mL^{-1} are considered promising. For crude extracts, the MIC should be ≤ 125 µg mL^{-1} [48]. The extract made known poor inhibitory activity against *Mycobacterium tuberculosis*, exhibiting a MIC and a Minimal Bactericidal Concentration (MBC) of 1250 and 2500 µg mL^{-1} respectively.

Computational results of compound 2

The structure of compound **2** was assigned based on spectroscopic analyses including, UV, IR, ^{1}H- and ^{13}C-NMR, 1D and 2D techniques. To get supplementary detailed awareness into the structure, DFT calculations were completed. The structure of the compound with the right stereochemistry was firstly optimized at B3LYP method using 6-31G(d) basis set and the optimized

structure was submitted to a relaxed scan around one H–C(5)–N(6)–H dihedral angle. Secondly, an additional relaxed scan around the other H–C(5)–N(6)–H dihedral angle (with no change in basis set) was applied on a conformer with low energy got from the preceding step. The desired conformer still with low energy was thereafter subjected to two relaxed scans around the C(5)–N(6)–C(7)–N(6) dihedral angles. All these scans led to an optimized geometry for **2**, based on the *cis*-relationship between H–C(5)–N(6)–H ($^3 J$(H,H) = 2.0 Hz). It is shown in Fig. 4 and takes in account previous reports on **1** [44, 49]. The five membered ring is almost planar as observed in the case of allantoin (**1**) [19].

The HOMO and LUMO of compound **2** (Fig. 5) as other descriptors were analyzed at B3LYP/6-31G(d) and 6-311G++(d,p) and compared with those of allantoin (**1**). The calculated HOMO–LUMO gap was 6.209 eV; results are summarized in Table 3.

The ^{1}H- and ^{13}C-NMR spectra of compound **2** were experimentally measured in DMSO-d_6 on 500 and 125 MHz spectrometers respectively. The theoretical NMR were calculated at B3LYP/6-31G(d,p) and MPW1PW91/6-31+G(d,p) in DMSO. The chemical shifts were also simulated at B3LYP/6-31G(d), B3LYP/6-31+G(d,p), MPW1PW91/6-31G(d) and MPW1PW91/6-31G(d,p); however, the correlation with the experiment was relatively weak. GIAO (Gauge Invariant Atomic Orbital) formalism was used during these calculations, and the solvent effect was introduced through polarizable continuum model (PCM) by applying integral equation formalism (IEF). A comparison of the theoretical ^{13}C-NMR values at B3LYP/6-31G(d,p) and MPW1PW91/6-31+G(d,p) with the experimental ones is given in Table 4. A better correlation with the experiment can be achieved if a scaling factor is applied to the ^{13}C-NMR theoretical values.

UV–visible spectrum of **1** displayed three maxima at λ_{max} 183, 195 nm (representing the absorption bands of amide and imide functions) [19] and 265 nm [44]. Despite on the fact that batesiin (**2**) is characterized by the same chromophore groups, its UV–visible spectrum (Fig. 2) exhibits one major absorption band at $\lambda_{max} = 296$ nm and minor absorptions as shoulder sections (letters A and B) with λ_{max} around 287 and 304 nm respectively. Simulated UV–visible spectra of **2** were achieved at B3LYP/6-31+G(d,p) with chloroform (non-polar aprotic solvent) and ethanol (polar protic solvent) (Fig. 6), based on its tautomeric and ionic forms (Fig. 7): all λ_{max} results (experimental and theoretical) are summarized in Table 5. Excitation energy (in nm) determined in CHCl$_3$ at 283.89 is closed to experimental value at 287 nm while simulation in EtOH exhibits an energy (in nm) at 315.59 which is comparable to the experimental λ_{max} at 304 nm.

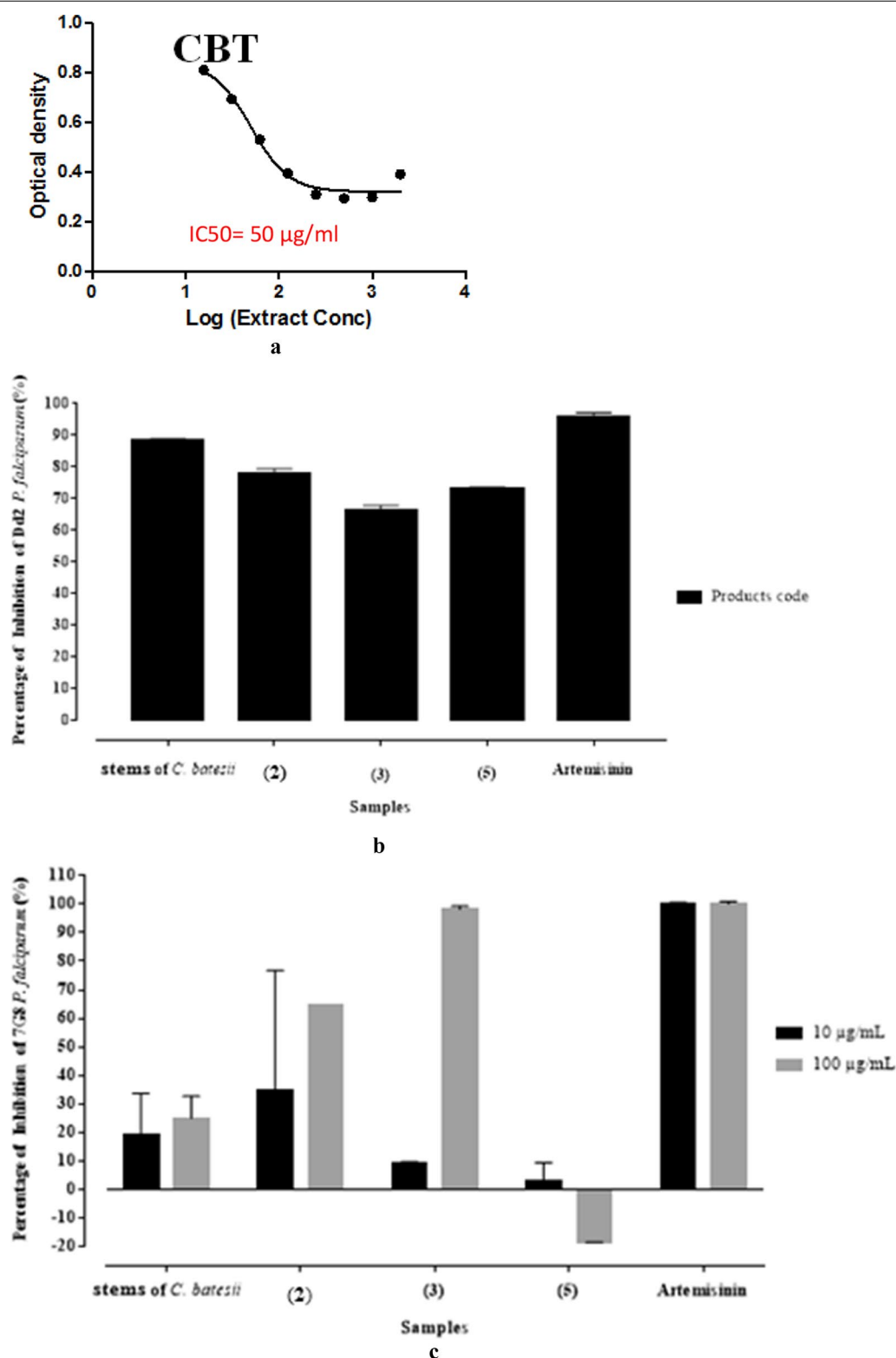Tiam *et al. BMC Chemistry*   (2021) 15:15

Page 7 of 17

Fig. 3 Result of twofold dose response analysis of the extract of *C. batesii* against Dd2 *P. falciparum* strain (**a**). Inhibition percentage of stems of *C. batesii* and isolated compounds against *P. falciparum* Dd2 strain (**b**). Inhibition percentage of stems of *C. batesii* and isolated compounds against *P. falciparum* 7G8 strain (**c**)

Table 2 MIC and MBC values of the methanol extract and the mixture of fatty acids (A$_1$) against *Mycobacterium tuberculosis* (AC 45)

Plant species	MIC[a] (µg mL^{-1})	MBC[b] (µg mL^{-1})	MBC/MIC
C. batesii	1250	2500	2
A$_1$	9.52	38.25	4
RMP	0.97	7.81	8

RMP Rifampicin

[a] Minimum inhibitory concentration

[b] Minimum bactericidal concentration

It must also be precised that results of IR calculations were almost similar to previous ones regarding allantoin (**1**) [19], since **1** and **2** share the same functional groups; hence, there was no need to report them.

Discussion

NMR data summarized in Table 3 strengthen the close relationship between allantoin (**1**) and batesiin (**2**), their ^{13}C chemical shifts being almost analogous (Table 1). The main difference relies on ^{1}H NMR spectra of both compounds: in **1**, a value at δ$_H$ 5.23 (1H, H–C(5)) ppm [50] is equivalent to chemical shift in **2** at δ$_H$ 5.30 (2H, d, ^3J(H,H) = 2.0 Hz, H–C(5)) ppm. This 0.7 ppm variation between the aforesaid chemical shifts could be explained by the conformation of **2** (Fig. 4b, c) which seems to induce deshielding of the hydrogen atoms located on carbons C(5).
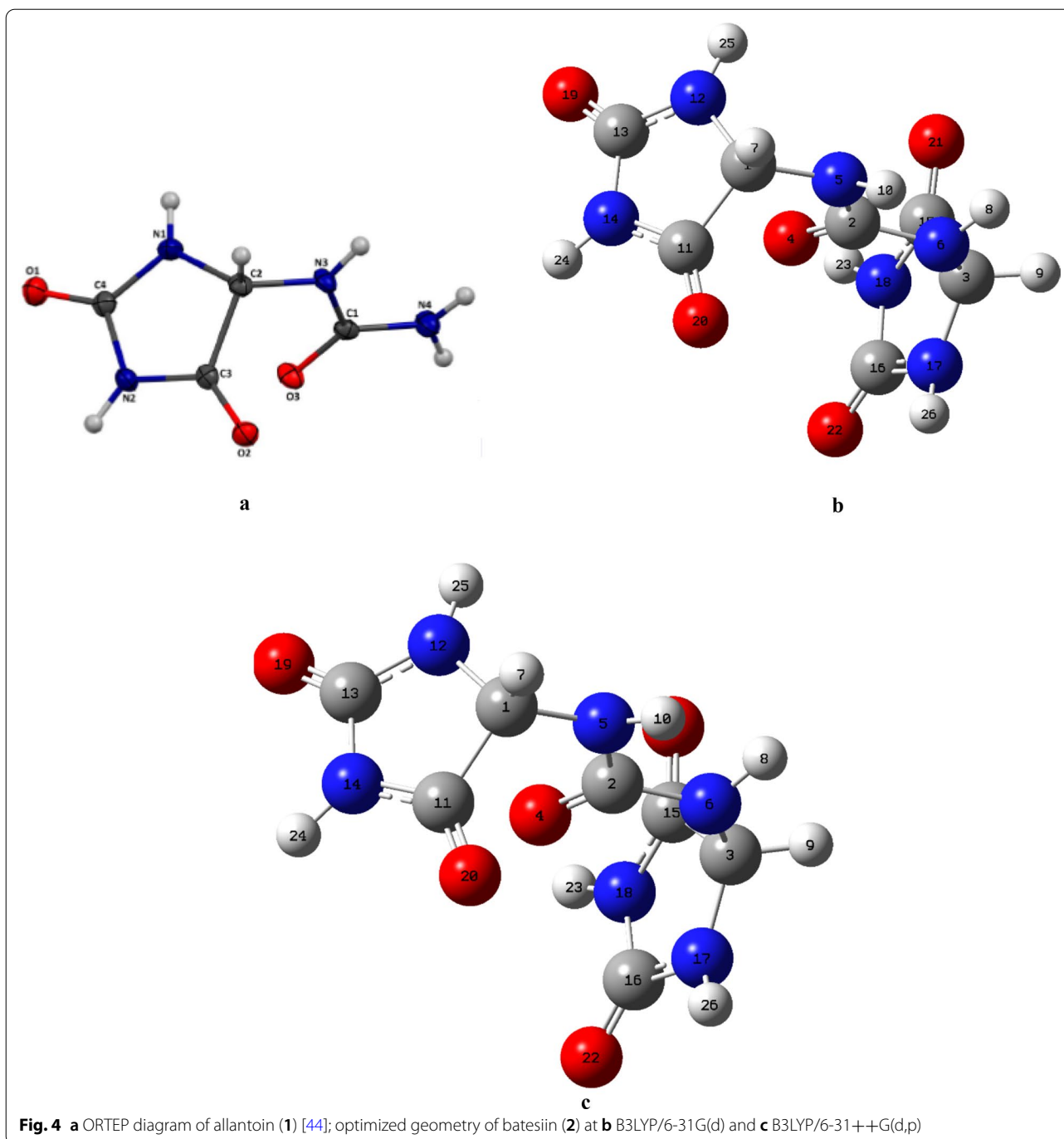
Results from bioassays against 7G8 *P. falciparum* strain reveal that an increase in concentration (10 to 100 µg mL^{-1}) marks an increase in percentages of inhibition for MeOH extract, **2** and **3**, but a decrease (with a negative percentage) for **5**, which should indicate that the latter is totally inactive at high concentrations. The moderate activity of the MeOH extract suggests insufficient synergistic or additive effects of potential antiplasmodial secondary metabolites from *C. batesii*. In contrast to the mixture of FA, the weak antimycobacterial properties of the crude extract suggest the occurrence within *C. batesii* of components with very poor antimycobacterial effects (Table 2). Moreover, a report from literature indicates that mycobacteria have a lipid-rich hydrophobic cell wall and are often susceptible to less polar compounds [51]. According to Peterson and Shanholtzer [52], bacteriostatic activity has been defined as a ratio of MBC to MIC of > 4. Hence, essential oil exhibited bacteriostatic activity.

The high value of the HOMO–LUMO band gap is indicative of a relative stability of the molecule towards oxidation–reduction reactions. However, it is less than the HOMO–LUMO band gap of allantoin (**1**) (see

Table 3) at the same method, maybe as an expression of additional stability of **2** and difference in biological behavior between both chemical entities. Plots of frontier orbitals show that HOMOs and LUMOs are globally focused over the entire molecule. Meanwhile, in the case of HOMOs, the ureidyl moiety is less concerned by the orbital overlap whereas it is recognized as the area covering the positive phase in LUMOs (Fig. 5). The theoretical ^{13}C-NMR values are, on the average, higher than the experimental ones when using MPW1PW91/6-31+G(d,p); by contrast, it is not the same observation with results provided by the B3LYP/6-31G(d,p) process. Regardless of the difference in the absolute values, the theoretical values match nicely with the experimental data. Based on the simulated UV–visible spectrum, batesiin (**2**) should most likely appear as an intermediate between various iminols and iminolates groups, precisely due to additional stability as already hypothesized (Fig. 8). Two free protons are supposed to be located somewhere between, in each case, a nitrogen and an anionic oxygen of the same iminolate group, at a site however nearer to oxygen (distance < 1.4 Å) than to nitrogen (distance > 2.3 Å) (Fig. 8). Hence, a virtual loss of symmetry becomes noticeable within **2**, inducing a change in MOs with an impact on electronic transitions (Fig. 9). LUMO and LUMO + 1 are localized on one imidazole fragment (especially in the region covering a free proton and the anionic oxygen located in its neighborhood) when the other one looks totally unoccupied. Moving from HOMO-1 to HOMO-3 causes an increase in orbital overlap within the entire chemical entity. Table 5 expresses the nature of electronic transitions which are in agreement with the corresponding λ$_{max}$, depending on the nature of the solvent.

Conclusion

Batesiin (**2**) has been characterized for the first time by means of ^{1}H-, ^{13}C-NMR and UV spectroscopies; its structure was confirmed by DFT and TD-DFT calculations at B3LYP/6-31G(d,p), 6-31G+(d,p), 6-311G++(d,p) and MPW1PW91/6-31G+(d,p) from this study. The MeOH crude extract of the stems showed a moderate activity against Dd2 *P. falciparum* strain with IC$_{50}$ = 50 µg mL^{-1}. The antiplasmodial properties of **2** and some other compounds are deduced from high percentages of growth inhibition against the 7G8 *P. falciparum* strain; in parallel, antimycobacterial activities against *M. tuberculosis* arise from the essential oil equivalent to the mixture of FA (**9–14**) with a MIC = 9.52 µg mL^{-1}. Additional data corresponding to HOMO, LUMO, enthalpy, entropy or some reactivity descriptors like *IP* or *EA* were also simulated, this time at B3LYP/6-31G(d) and 6-311G++(d,p) and compared with data from literature of allantoin (**1**)

Fig. 4 **a** ORTEP diagram of allantoin (**1**) [44]; optimized geometry of batesiin (**2**) at **b** B3LYP/6-31G(d) and **c** B3LYP/6-31++G(d,p)
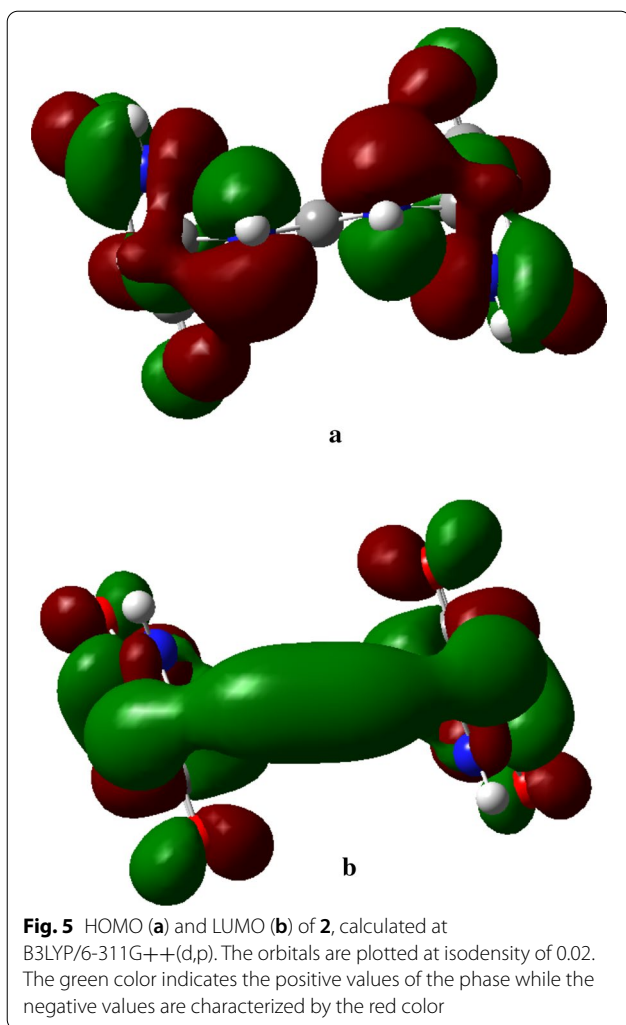
[19]; moreover, no comparison with the experiment in this case could be made. This work supports a good agreement between experimental data and DFT calculations in case of structure elucidation. These preliminary results also support the hypothesis of further development of new antimalarial and antitubercular drugs from the genus *Cordia*.

Methods

General

Melting points were uncorrected and were measured on a Mettler Toledo instrument. IR spectra were recorded on an Alpha II FT-IR spectrometer from Bruker in the region of 4000–600 cm^{-1}, using KBr pellet technique with 1.0 cm^{-1} resolution at room temperature. 1D and 2D NMR spectra were obtained on a

Tiam *et al. BMC Chemistry*   (2021) 15:15

Page 10 of 17

Fig. 5 HOMO (**a**) and LUMO (**b**) of **2**, calculated at B3LYP/6-311G++(d,p). The orbitals are plotted at isodensity of 0.02. The green color indicates the positive values of the phase while the negative values are characterized by the red color

Bruker DRX 500 (500 MHz for ^{1}H and 125 MHz for ^{13}C spectra) spectrometer (Bruker, Rheinstetten, Germany) with chemical shifts reported as δ (ppm), using TMS as an internal standard. The ESI-MS were obtained on LTQ-FT instrument (Thermo Scientific). LC–MS were measured with Shimadzu LC–MS system using a L-column 2 ODS (I.D. 2.1 × 100 mm, Chemical Evaluation and Research Institute, Japan), at a flow rate of 0.2 mL min^{-1} with a detection wavelength of 300 nm and FMW (HCOOH/MeCN/H$_2$O = 1:12:87) as eluent, ESI+ 4.5 kV, ESI− 3.5 kV, 250 °C. Optical rotations were measured on a Perkin-Elmer 341 polarimeter. Silica gel 60 (230−400 mesh E. Merck, Darmstadt, Germany) and *Sephadex*® LH-20 were employed for CC, the solvent mixing systems for elution were mainly CH$_2$Cl$_2$/MeOH for the phytochemical study with increasing polarity and pure MeOH, while precoated aluminum sheets silica gel 60 F254 were used for TLC [53].

Plant material

The plant material was collected on March 2014 at Koumoul in center region of Cameroon. The identity of plant material was confirmed by the taxonomist Victor Nana. A voucher sample (14,106 SRF) is deposited at the National Herbarium of Cameroon, Yaounde.

Extraction and isolation

The stems were dried in shade and cut into small pieces and then submitted for further studies. 80% of air dried pieces of stems of *C. batesii* (500 g) were extracted with MeOH (5 × 500 mL, 30 min each) using an Elma® sonic S 100 at r. t. The extract was filtered; the filtrate was evaporated to dryness in a Rotavapor. The residue obtained from the MeOH extract (about 53 g) was dissolved into hexane−water 80:20 (100 mL) during 1 day; the resulting hexane−water gum (42 g) was dissolved in a mixture of CHCl$_3$−H$_2$O 80:20 (100 mL) once again in a period of 24 h; the resulting CHCl$_3$−H$_2$O extract (36 g) was dissolved in CH$_3$COOH−H$_2$O 70:30 (100 mL) during 24 h. The final extract (26 g) was submitted to further CC analyses. The crude MeOH extract (26 g) was subjected to CC of LH-20 (2.5 cm, 50 cm, eluent MeOH). Four main fractions were obtained: A (10.36 g), B (4.6 g), C (3.0 g) and D (7.0 g). Fraction A (10.36 g) was subjected to a silica gel CC (1.8 cm, 3 × 50 cm, eluent CH$_2$Cl$_2$−MeOH 100−1:1) and provided three subfraction (A$_1$, A$_2$, and A$_3$). Sub-fraction A$_2$ (5.20 g) was fractionated by silica gel CC (1.8 cm, 3 × 50 cm, eluent CH$_2$Cl$_2$−MeOH 50:1−30:1) to produce two compounds, **4** (4.6 mg) and **5** (11 mg). Fraction B (4.6 g) was chromatographed as described above to give five sub-fractions (B$_1$, B$_2$, B$_3$, B$_4$ and B$_5$). Sub-fraction B$_1$ (0.20 g) was purified by silica gel CC (1.8 cm, 3 × 50 cm, eluent CH$_2$Cl$_2$−MeOH 30:1−20:1) to yield compound **1** (9 mg). Compound **2** (7.5 mg) was isolated from sub-fraction B$_3$ (0.31 g) using a silica gel CC (1.8 cm, 3 × 50 cm, eluent CH$_2$Cl$_2$−MeOH 40:1−20:1). Sub-fraction B$_4$ (0.60 g) was fractionated and purified using a silica gel CC (1.8 cm, 3 × 50 cm, eluent CH$_2$Cl$_2$−MeOH 40:1−15:1) to provide **3** (4 mg). The essential oil (sub-fraction A$_1$, 0.60 g) resulting from the crude extract was analyzed by LC–MS, exhibiting compounds **6**, **7** and **8**. A$_1$ was soluble in pure hexane and crystallized from pure CH$_2$Cl$_2$. 487 mg were analyzed by GC–MS which revealed the compounds **9**, **10**, **11**, **12**, **13** and **14**.

Characteristics of compound 2

Batesiin (**2**), white solid: mp 231−233 °C. TLC (CH$_2$Cl$_2$:MeOH, 20:1 v/v) R$_f$ = 0.6; $[\alpha]_D^{20}$ = − 98.3°

Tiam *et al. BMC Chemistry*   (2021) 15:15

Page 11 of 17

Table 3 Some electronic and thermodynamic results of batesiin (2) compared to data of allantoin (1) at B3LYP

Parameters	Allantoin (1) [19]	Batesiin (2)	
	B3LYP/6-311G++(d,p)	B3LYP/6-31G(d)	B3LYP/6-311G++(d,p)
SCF energy (a.u.)	− 600.96805371	− 976.275521823	− 976. 58,639,012
Zero point vibrational energy (kcal mol^{-1})	77.961	117.242	116.472
Rotational constants (GHz)	1.876	0.713	0.721
	0.876	0.262	0.257
	0.754	0.261	0.254
Rotational temperatures (Kelvin)	0.090	0.034	0.035
	0.042	0.013	0.012
	0.036	0.013	0.012
Total energy (thermal) (kcal mol^{-1})	84.462	127.176	126.495
Molar heat capacity at constant volume, c_v (cal mol^{-1} K^{-1})	37.756	58.872	59.237
Molar heat capacity at constant pressure, c_p (cal mol^{-1} K^{-1})	39.744	60.86	61.225
Total entropy, S (cal mol^{-1} K^{-1})	100.186	129.784	130.265
Total enthalpy, H (kcal mol^{-1})	85.055	127.769	127.088
Frontier MO energies (eV)			
E_{LUMO}	− 1.196	− 0.647	− 1.440
E_{HOMO}	− 7.456	− 7.149	− 7.649
E_{LUMO}−E_{HOMO}	6.260	6.502	6.209
Global reactivity descriptors			
Ionization potential, IP (eV)	7.456	7.149	7.649
Electron affinity, EA (eV)	1.196	0.647	1.440
Electronegativity, χ	4.326	3.898	4.544
Chemical potential, μ	− 4.326	− 3.898	− 4.544
Hardness, η	3.130	3.251	3.104
Softness, S	0.160	0.154	0.161

The values are calculated in gas phase (at 298.15 K)

(0.04 M in acetone). ^{1}H NMR (500 MHz, DMSO-d_6) δ 10.51 (2H, s, NH), 8.04 (2H, s, NH), 6.88 (2H, d, J = 2 Hz, NH), 5.23 (2H, d, J = 2 Hz); ^{13}C NMR (125 MHz, DMSO-d_6) δ 62.4, 156.8, 157.4, 173.6; IR (KBr) cm^{-1} 3425, 3340 (O–H), 3125, 3060 (N–H), 1810, 1740, 1680, 1560 (C=O); UV/Vis: λ$_{max}$ (MeOH) nm: 296. HR-LC/MS (m/z): [M+Na]$^+$ calcd for $C_7H_8N_6O_5Na^+$; 279.1608; found 279.1603; analysis (calcd., found for $C_7H_8N_6O_5Na$): C (30.12, 30.09); H (2.89, 2.85); N (30.10, 30.10); O (28.66, 28.65).

Table 4 Experimental and calculated [at B3LYP/6-31G(d,p) and MPW1PW91/6-31+G(d,p)] ^{13}C-NMR data of 1

Position	^{13}C chemical shifts (ppm)		
	Experimental	B3LYP/6-31G(d,p)	MPW1PW91/6-31+G(d,p)
2	156.8	156.1	157.0
4	173.6	174.4	174.6
5	62.4	61.7	62.7
7	157.4	157.0	158.0

Biological assays

In vitro cultivation of P. falciparum strains

*Pf*Dd2 and *Pf*7G8 strains of *P. falciparum* were used in vitro in blood stage culture to test the antimalarial efficacy of MeOH extract of stems of *C. batesii* and isolated compounds **2**, **3** and **5**. The culture was maintained at the Laboratory of parasitology, Centre Pasteur du Cameroon. *P. falciparum* culture was maintained according to the method described by Trager and Jensen [54] with slight modifications. *P. falciparum* Dd2 and 7G8 cultures were maintained in fresh O^{+ve} human erythrocytes suspended at 4% haematocrit in RPMI 1640 (Sigma Aldrich—France) containing 0.2% sodium bicarbonate, 0.5% Albumax, 45 μg L^{-1} hypoxanthine and 50 μg L^{-1} gentamicin, and incubated at 37 °C under a gas mixture 5% O$_2$, 5% CO$_2$, and 90% N$_2$. Every day, infected erythrocytes were transferred into fresh complete medium to propagate the culture.
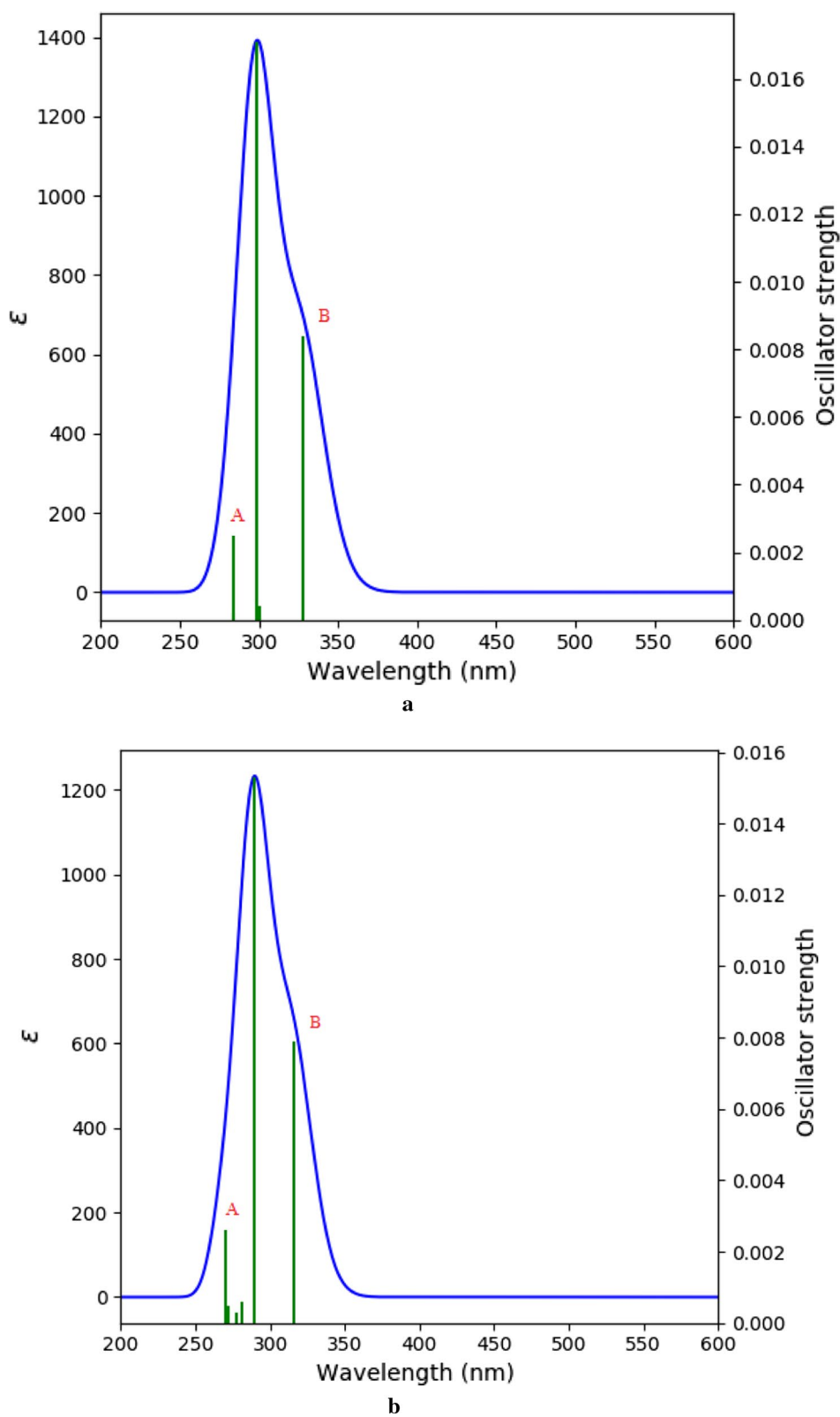
Tiam *et al. BMC Chemistry*   (2021) 15:15

Page 12 of 17

Fig. 6 UV–visible spectra of **2** in chloroform (**a**) and in ethanol (**b**), calculated at B3LYP/6-31G+(d,p)

Tiam *et al. BMC Chemistry*   (2021) 15:15
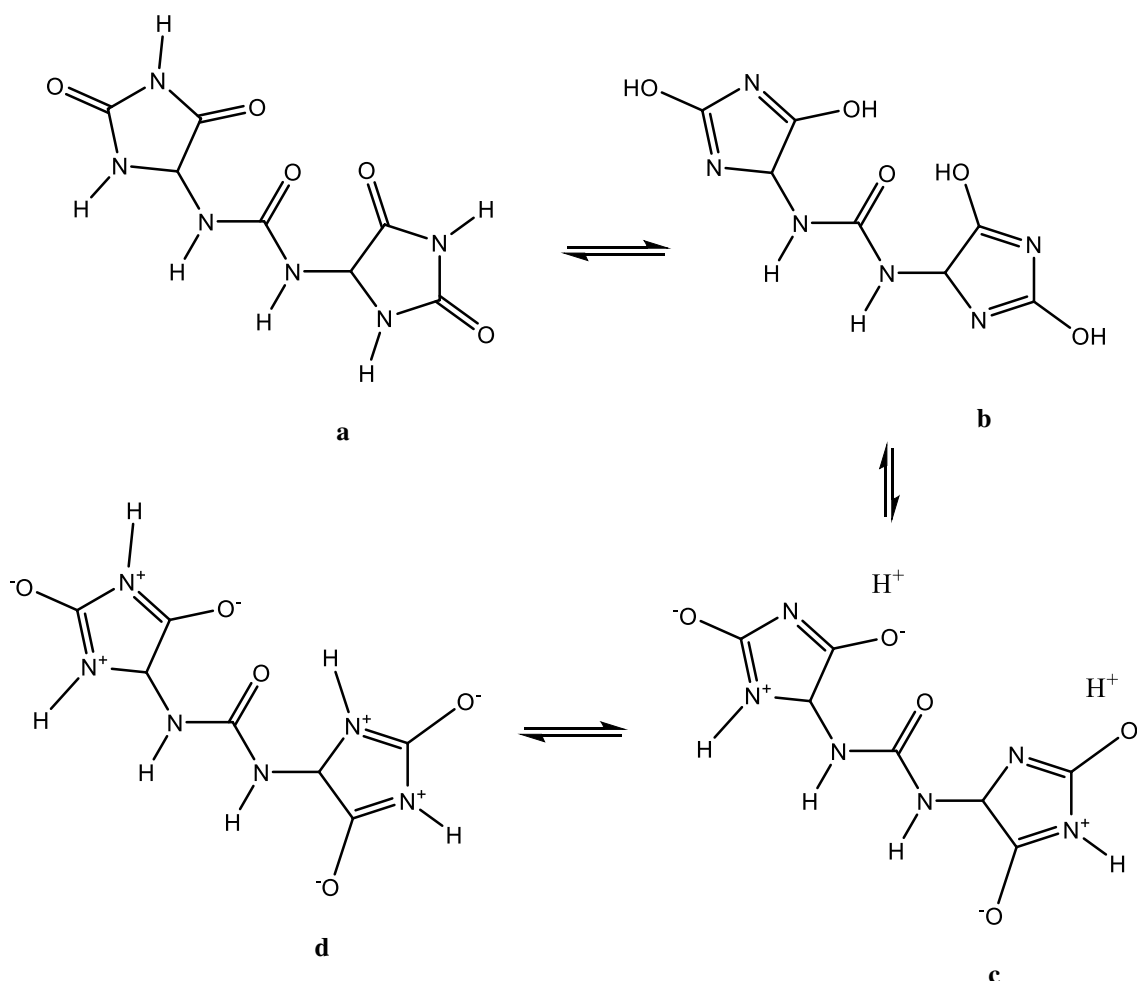
Page 13 of 17

Fig. 7 Tautomeric and ionic forms of **2**; based on UV–visible results, it seems most likely that the (**C**) form should be the major one

Table 5 Main experimental and vertical excitation energies of batesiin (2) along with oscillator strengths and transitions

Experimental	Excitation energy (nm)		Oscillator strength		Electronic transition	
	CHCl$_3$	EtOH	CHCl$_3$	EtOH	CHCl$_3$	EtOH
287	283.89	270.11	0.0025	0.0026	[a]H–2 → [b]L + 1	[a]H–2 → [b]L + 1
296	299.01	289.70	0.0171	0.0153	[a]H–3 → [b]L	[b]H–3 → [b]L
304	327.69	315.59	0.0084	0.0079	[a]H–1 → [b]L	[a]H–1 → [b]L

[a] H: HOMO

[b] L: LUMO

Drug dilutions

Artemisinin (Sigma Aldrich—France) and isolated compounds were prepared in DMSO. All stocks were then diluted with culture medium to achieve the required concentrations. The final solution of all plant extracts, isolated compounds and artemisinin contained 0.4% DMSO, which was found to be non-toxic

to the parasites. Drugs and test compounds were then placed in 96-well flat bottom tissue culture grade plates.

Assay for antiplasmodial activity

The stems of *C. batesii* were evaluated for their antimalarial activity against *P. falciparum* strains Dd2 and 7G8. For
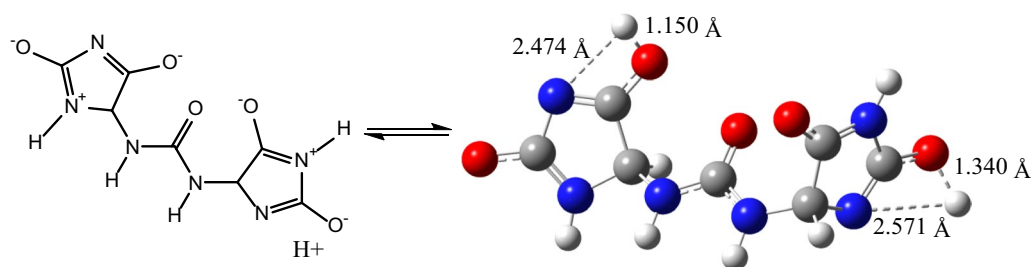
Tiam *et al. BMC Chemistry*   (2021) 15:15

Page 14 of 17

Fig. 8 One case of simulated "iminol"/"iminolate" form of **2** with distances between protons and nitrogen or oxygen atoms at B3LYP/6-31G+(d,p); this form seems to induce the electronic transitions (in nm)
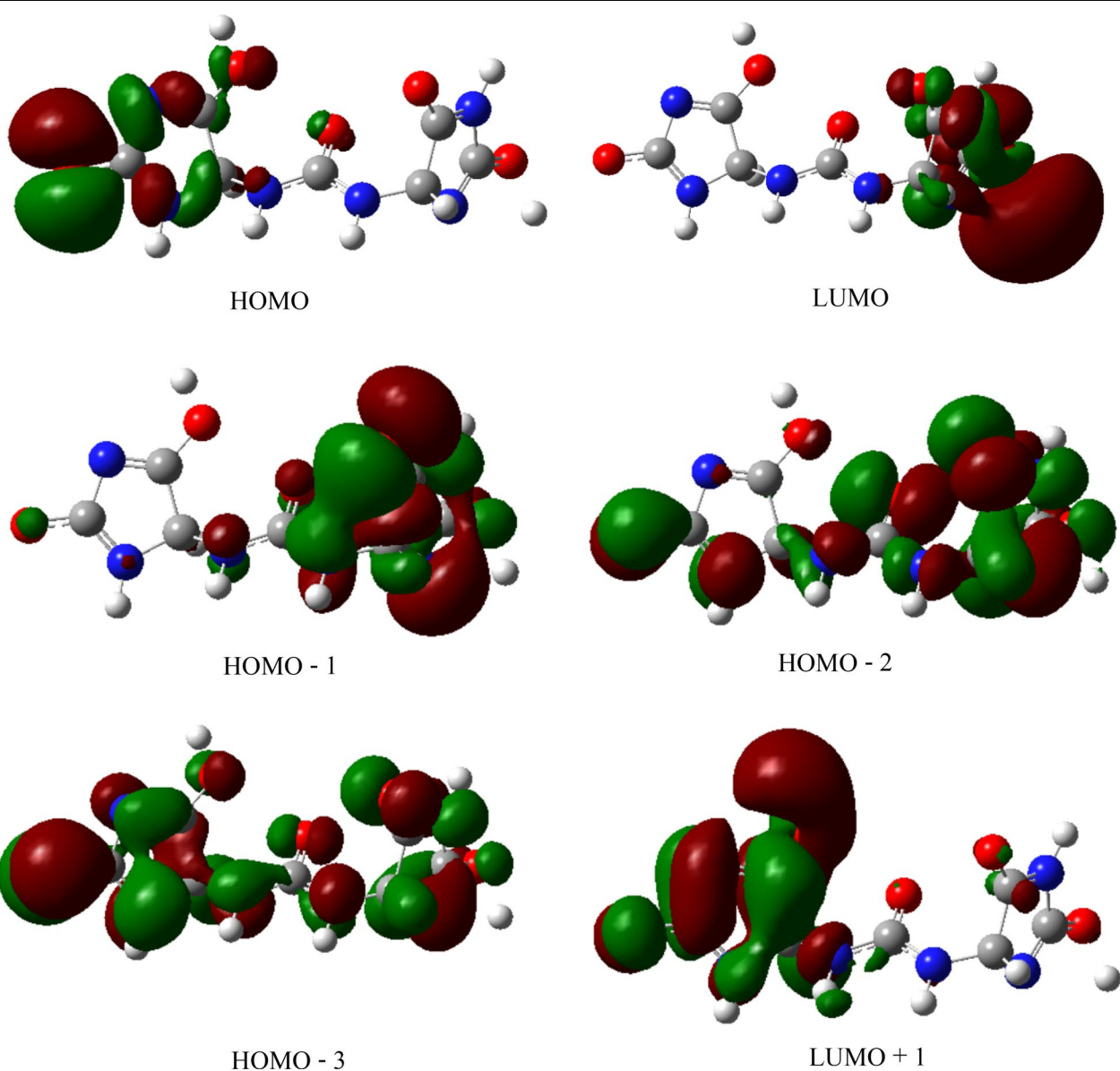

Fig. 9 Various MOs of **2** involved in electronic transitions, at B3LYP/6-31G+(d,p). The green color represents the positive values of the phase while the red color is indicative of its negative values

Tiam *et al. BMC Chemistry*   (2021) 15:15

Page 15 of 17

drug screening, SYBR green I-based fluorescence assay was setup as described by Smilkstein et al. [46]. Sorbitol synchronized parasites were incubated under normal culture conditions at 2% haematocrit and 1% parasitemia in the absence or presence of increasing concentrations of MeOH extracts of *C. batesii*. Artemisinin was used as positive control, while 0.4% DMSO was used as the negative control. After 48 h of incubation, 100 µL of SYBR Green I solution [0.2 µL mL^{-1} of 10,000× SYBR Green I (Sigma Aldrich—France)] in lysis buffer [Tris (20 mM; pH 7.5), EDTA (5 mM), saponin (0.008%; w/v) and Triton X-100 (0.08%; v/v)] was added to each well. The microtiter plate was mixed twice gently with multi-channel pipette and incubated in dark at 37 °C for 1 h. Fluorescence was measured with a fluorescence multi-well plate reader (Perkin Elmer) with excitation and emission wavelength bands centred at 485 and 530 nm, respectively. The fluorescence counts were plotted against the drug concentration and the inhibitory percentage of each plant extract and compound was calculated using the following equation:

$$I(\%) = \frac{Abs_{control} - Abs_{extracts/isolated\ compounds}}{Abs_{control}} \times 100$$

where $Abs_{control}$ is the absorbance of untreated well and $Abs_{extracts/isolated\ compounds}$ is the absorbance of extracts or compounds well.

Antimycobacterial tests

For the present study, the mycobacterium (*M. tuberculosis*) used was a clinical isolated strain resistant to isoniazid codified as AC 45 (this strain was obtained from Sangmelima district's Hospital in south region of Cameroon). The genetical profile of the resistance has been carried out at Laboratory for Tuberculosis Research (Biotechnology Centre, University of Yaoundé I) through Line probe Assay method. The mycobacteria strains have been cultured at 37 °C for 2 weeks in Middlebrook 7H9 (Himedia, India) supplemented with 0.05% (v/v), 2% glycerol and 10% OADC (oleic acid-albumin-dextrose-catalase of Liofilchem s.r.l, Italia). The optical density of 0.45 to 0.55 was measured using spectrophotometer at 550 nm to obtain a suspension of 1.5×108 UFC mL^{-1}. The activity of all phytochemicals (extract and pure compounds) against the aforementioned *M. tuberculosis* strains was tested using the microplate Alamar Blue assay as described previously by Collins and Franzblau [55]. In a 96 well microplates, all wells received 100 µL of supplemented Middlebrook 7H9 broth, then working metabolites solutions (100 µL) were poured into the first well of each row, from which twofold dilution series were made through the microplate column. The test inoculum (100 µL) was added to all testing wells, as well as to the drug-free control wells. The final concentration of DMSO in wells was 7% v/v. The final concentrations tested ranged from 250 to 0.244 µg mL^{-1} for pure compounds and 5000 to 4.882 µg mL^{-1} for extracts. Rifampicin was used as standard drug. Each concentration was assayed in triplicate. Each microplate was sealed with parafilm paper and incubated for 14 days at 37 °C. After that, 40 µL of Alamar blue solution was added to two columns of each triplicate in order to show mycobacterial growth and the plates were re-incubated at 37 °C for 24 h. After 1 day of incubation, the MIC was defined as the lowest concentration of phytochemicals that inhibited the bacterial growth (prevents a color change from blue to pink) after incubation time [56]. For the MBC determination, 50 µL of each well which concentration was $\geq$ MIC was sub-cultured in 150 µL of Mbk 7H9 medium and incubated at 37 °C for 10 days, then mycobacterial growth was carried out by addition of 40 µL of alamar blue. MBC was defined as the lowest concentration of extract at which no visible growth of the germ was observed.

Computational details

All calculations were performed with Gaussian 09 suite of programs [57] and UV–visible curves were generated by GaussSum [58]. Geometries were optimized at hybrid B3LYP method using 6-31G(d) basis set. The B3LYP mode provides a good balance between cost and precision [59, 60]. A preliminary predict of the geometry of compound **2** is based on the stereochemistry ascribed through 1D and 2D NMR characterizations. Compound **2** has conformational flexibility around the symmetric dihedral angles H−C(5)−N(6)−H and C(5)−N(6)−C(7)−N(6). The dihedral angles around the C(5)−N(6) axes were scanned at 15 degrees step and a minimum at 22.9° around the C(5)−N(6) axes was retained because of its conformation closed to the structure of allantoin (**1**). Afterwards, dihedral angles around the N(6)−C(7) axes were scanned at 10 degrees step, to find the lowest energy conformer. It was then submitted to geometry optimization at B3LYP/6-31G(d) and B3LYP/6-311++G(d,p) levels of theory to provide the optimized geometries of **2** (Fig. 4). The optimized structure was in each case confirmed by frequency analysis at the same levels as a true minimum (no imaginary frequency). Six methods were evaluated for the simulation of ^{1}H- and ^{13}C-NMR spectra; B3LYP/6-31G(d),   B3LYP/6-31G(d,p),   B3LYP/6-31G+(d,p), MPW1PW91/6-31G(d),MPW1PW91/6-31G(d,p)andMPW 1PW91/6-31G+(d,p). The electronic properties at isodensity 0.02 such as Ionization Potential (*IP*), Electron Affinity (*EA*), HOMO, LUMO and band gaps were calculated at B3LYP/6-31G(d) and B3LYP/6-311G++(d,p).

Tiam *et al. BMC Chemistry*   (2021) 15:15

Page 16 of 17

The band gap was taken as the difference in energies of HOMO and LUMO. Meantime, thermodynamic properties like enthalpy, entropy or molar capacity at constant volume along with reactivity descriptors like chemical potential, electronegativity, hardness, softness were also calculated by means of the same methods. TD-DFT studies were evaluated at B3LYP/6-31G+(d,p) in CHCl$_3$ and in EtOH after a geometry optimization at the same level of theory of the iminolate in Fig. 8. Six steps were applied to get excitation energies.

Supplementary Information
The online version contains supplementary material available at https://doi.org/10.1186/s13065-021-00742-5.

Additional file 1. NMR spectra of compound **2**, some HMBC correlations, GC–MS analyses of compounds **9**, **10**, **11**, **12**, **13** and **14**, LC–MS and GC–MS chromatograms of the extract of *C. batesii*, the ESI-MS spectrum of compound **2**, the genotype profile of *M. tuberculosis* codified AC 45, the shielding tensors of the nuclei of **2**, the electronic (HOMO, LUMO) properties, the cartesian coordinates of the optimized geometry of compound **2** and TD-DFT are available as additional file.

Authors' contributions
ERT, NMN and PHBD performed the experiments, DSNB, IMN and AAAZ analyzed the data, conceived and designed the experiments and wrote the article. LA, BLN, JNM and DEP, contributed samples/reagents/materials/analysis tools and analyzed the data. All authors read and approved the final manuscript.

Availability of data and materials
All data generated or analyzed during this study are included in this published article (and its Additional file 1).

Declarations

Ethics approval and consent to participate
Not applicable.

Consent for publication
Not applicable.

Competing interests
The authors declare that they have no competing interests.

Author details
[1] Department of Organic Chemistry, Faculty of Science, University of Yaoundé I, P.O Box 812, Yaounde, Cameroon. [2] Department of Inorganic Chemistry, Faculty of Science, University of Yaoundé I, P.O Box 812, Yaounde, Cameroon. [3] Department of Chemistry, Higher Training College, University of Yaoundé I, P.O Box 47, Yaounde, Cameroon. [4] Centre Pasteur du Cameroun, Yaounde, Cameroon. [5] Centre for Research on Medicinal Plants and Traditional Medicine, Institute of Medical Research and Medicinal Plants Studies, Yaounde, Cameroon.

References
1. World Health Organization. Accelerating progress on HIV, tuberculosis, malaria, hepatitis and neglected tropical diseases: a new agenda for 2016–2030. 2015. World Health Organization. https://apps.who.int/iris/handle/10665/204419. Accessed 15 Sept 2020.
2. Rasmussen C, Nyunt MM, Ringwald P (2017) Artemisinin-resistant *Plasmodium falciparum* in Africa. N Engl J Med 377:305–306
3. Houben RM, Dodd PJ (2016) The global burden of latent tuberculosis infection: a re-estimation using mathematical modelling. PLoS Med 13:e1002152
4. Der Meeren OV, Hatherill M, Nduba V, Wilkinson RJ, Muyoyeta M, Van Brakel E et al (2018) Phase 2b controlled trial of M72/AS01E vaccine to prevent tuberculosis. N Engl J Med 379:1621–1634
5. World malaria report. Geneva: World Health Organization; 2019. Licence: CC BY-NC-SA 3.0 IGO.
6. Romero JA, Acosta ME, Gamboa ND, Mijares MR, De Sanctis JB, Llovera LJ, Charris JE (2019) Synthesis, antimalarial, antiproliferative, and apoptotic activities of benzimidazole-5-carboxamide derivatives. Med Chem Res 28:13–27
7. Al-Otaibi JS, Almuqrin AH, Mary YS, Thomas R (2020) Modeling the conformational preference, spectroscopic properties, UV light harvesting efficiency, biological receptor inhibitory ability and other physico-chemical properties of five imidazole derivatives using quantum mechanical and molecular mechanics tools. J Mol Liq 310:112871–112875
8. Lodewyk MW, Siebert MR, Tantillo DJ (2012) Computational Prediction of ^{1}H and ^{13}C chemical shifts: a useful tool for natural product, mechanistic, and synthetic organic chemistry. Chem Rev 112:1839–1862
9. Oza MJ, Kulkarni YA (2017) Traditional uses, phytochemistry and pharmacology of the medicinal species of the genus *Cordia* (Boraginaceae). J Pharm Pharmacol 69:755–789
10. Barroso ICE, de Oliveira F, Ciarelli DM (2009) Morphology of the dispersion unit and germination of *Cordia sellowiana* and *Cordia myxa*. Bragantia 68:241–249
11. Ioset JR, Marston A, Gupta MP, Hostettmann K (2000) Antifungal and larvicidal compounds from the root bark of *Cordia alliodora*. J Nat Prod 63:424–426
12. Marston A, Zagorski MG, Hostettmann K (1988) Antifungal polyphenols from *Cordia goetzei*. Helv Chim Acta 71:1210–1217
13. Hernandez T, Canales M, Teran B, Avila O, Duran A, Garcia AM et al (2007) Antimicrobial activity of the essential oil and extracts of *Cordia curassavica* (Boraginaceae). J Ethnopharmacol 111:137–141
14. Okusa PN, Penge O, Devleeschouwer M, Duez P (2007) Direct and indirect antimicrobial effects and antioxidant activity of *Cordia gilletii* De Wild (Boraginaceae). J Ethnopharmacol 112:476–481
15. Jamkhande PG, Ghante MH, Barde SR, Ajgunde BR (2019) Antimycobacterial, antimicrobial, antioxidant activities and *in silico* PASS investigations of root fractions and extract of *Cordia dichotoma*. Orient Pharm Exp Med 19:485–496
16. Tracey MV (1955) Urea and ureides. In: Paech K, Tracey MV (eds) Modern methods of plant analysis. Springer, Berlin, pp 119–141
17. da Silva VC, de Carvalho MG, Alves AN (2008) Chemical constituents from leaves of *Palicourea coriacea* (Rubiaceae). J Nat Med 62:356–357
18. Kus N, Bayar SH, Fausto R (2009) Thermal decomposition of allantoin as probed by matrix isolation FTIR spectroscopy. Tetrahedron 65:9719–9727
19. Alam MJ, Ahmad S (2015) FTIR, FT-Raman, UV–visible spectra and quantum chemical calculations of allantoin molecule and its hydrogen bonded dimers. Spectrochim Acta A 136:961–978
20. Nariya PB, Shukla VJ, Acharya RN, Nariya MB, Dhalani JM, Patel AS, Ambasana PA (2018) Triterpenoid and fatty acid contents from the stem bark of *Cordia dichotoma*. Folia Med (Plovdiv) 60:594–600
21. McKinney JD, Höner zu Bentrup K, Muñoz-Elías EJ, Miczak A, Chen B, Chan WT, Swenson D, Sacchettini JC et al (2000) Persistence of *Mycobacterium*

Tiam *et al. BMC Chemistry*   (2021) 15:15

Page 17 of 17

tuberculosis in macrophages and mice requires the glyoxylate shunt enzyme isocitrate lyase. Nature 406:735–738

22. Arai M, Yamano Y, Kamiya K, Setiawan A, Kobayashi M (2016) Anti-dormant mycobacterial activity and target molecule of melophlins, tetramic acid derivatives isolated from a marine sponge of *Melophlus* sp. J Nat Med 70:467–475

23. Lawal TO, Mbanu AE, Adeniyi BA (2014) Inhibitory activities of *Ceibapentandra* (L.) Gaertn and *Cordiasebestena* Linn. on selected rapidly growing mycobacteria. Afr J Microbiol Res 28:2387–2392

24. Dai J, Sorribas A, Yoshida WY, Williams PG (2010) Sebestenoids A-D, BACE1 inhibitors from *Cordia sebestena*. Phytochemistry 71:2168–2173

25. Rekha M, Kowsalya M (2020) A new organic dye *Cordia sebestena* sensitized solar cell with current-voltage characteristics. Asian J Chem 32:342–348

26. Aayisha S, Devi TSR, Janani S, Muthu S, Raja M, Sevvanthi S (2019) DFT, molecular docking and experimental FT-IR, FT-Raman, NMR inquisitions on "4-chloro-*N*-(4,5-dihydro-1*H*-imidazol-2-yl)-6-methoxy-2-methylpyrimidin-5-amine": alpha-2-imidazoline receptor agonist antihypertensive agent. J Mol Struct 1186:468–481

27. Zhou CX, Jian-Xia Mo JX, Wang XY, Zhang J, Gan LS (2011) Theoretical study on flueggenines A and B: a comparison of calculated spectroscopic properties with IR, UV and ECD experimental data. J Mol Struct 989:131–135

28. Becke DA (1993) Density-functional thermochemistry. III. The role of exact exchange. J Chem Phys 98:5648–5652

29. Lee C, Yang W, Parr RG (1988) Development of the Colle-Salvetti correlation-energy formula into a functional of the electron density. Phys Rev B 37:785–789

30. Adamo C, Barone V (1998) Exchange functionals with improved long-range behavior and adiabatic connection methods without adjustable parameters: the *m*PW and *m*PW1PW models. J Chem Phys 108:664–675

31. Perdew JP, Chevary JA, Vosko SH, Jackson KA, Pederson MR, Singh DJ, Fiolhais C (1992) Atoms, molecules, solids, and surfaces: applications of the generalized gradient approximation for exchange and correlation. Phys Rev B 46:6671–6687

32. Zeukang RD, Noundou XS, Fotsing MT, Kuiate TT, Mbafor JT, Krause RWM et al (2019) Cordidepsine is a potential new anti-HIV depsidone from *Cordia millenii*. Molecules 24:3202–3216

33. Li P, Feng ZX, Ye D, Huan W, Gang WD, Dong LX (2003) Chemical constituents from the whole plant of *Euphorbia altotibetic*. Helv Chim Acta 86:2525–2532

34. Velde VV, Lavie D, Zelnik R, Matida AK, Panizza S (1982) Cordialin A and B, two new triterpenes from *Cordia verbenacea*. J Chem Soc Perkin Trans 1:2697–2700

35. Formica JV, Regelson W (1995) Review of the biology of quercetin and related bioflavonoids. Food Chem Toxicol 33:1061–1080

36. Hergert HL (1956) The flavonoids of lodgepole pine bark. J Org Chem 21:534–537

37. Coughlin JL, Winnik B, Buckley B (2011) Measurement of bisphenol A, bisphenol A β-D-glucuronide, genistein, and genistein 4′-β-D-glucuronide via SPE and HPLC–MS/MS. Anal Bioanal Chem 401:995–1002

38. Deliy IV, Vlasova EN, Nuzhdin AL, Gerasimov EY, Bukhtiyarova GA (2014) Hydrodeoxygenation of methyl palmitate over sulfided Mo/Al$_2$O$_3$, CoMo/Al$_2$O$_3$ and NiMo/Al$_2$O$_3$ catalysts. RSC Adv 4:2242–2250

39. Gao H, Hong K, Zhang X, Liu HW, Wang NL, Zhuang L, Yao XS (2007) New steryl esters of fatty acids from the mangrove fungus *Aspergillus awamori*. Helv Chim Acta 90:1165–1178

40. El-Shouny WA, Ali SS, Sun J, Samy SL, Ali A (2018) Drug resistance profile and molecular characterization of extended spectrum beta-lactamase (ESβL)-producing *Pseudomonas aeruginosa* isolated from burn wound infections; essential oils and their potential for utilization. Microb Pathog 116:301–312

41. Kazi SA, Clark P, Campi EM, Jackson WR, Hearn MTW (2019) Metathesis reactions with a low-cost spinning disk system. Green Chem Lett Rev 12:407–419

42. Azuma CM, dos Santos FCS, Lago JHG (2011) Flavonoids and fatty acids of *Camellia japonica* leaves extract. Braz Pharmacogn 21:1159–1162

43. Nie Y & Stürzenbaum SR. Model nematodes. In: Obesity research in animal models for the study of human disease. 2nd edn. Amsterdam: Elsevier Inc; 2017. p. 267–80.

44. Lakshmanan G, Sivaraj C, Ammar A, Krishnan DA, Gopinath S, Saravanan K et al (2019) Isolation and structural elucidation of allantoin, a bioactive compound from *Cleome viscosa*: a combined experimental and computational investigation. Pharmacogn J 11:1391–1400

45. Fulmer GR, Miller AJM, Sherden NH, Gottlieb HE, Nudelman A, Stoltz BM et al (2010) NMR chemical shifts of trace impurities: common laboratory solvents, organics, and gases in deuterated solvents relevant to the organometallic chemist. Organometallics 29:2176–2179

46. Smilkstein M, Sriwilaijaroen N, Kelly JX, Wilairat D, Riscoe M (2004) Simple and inexpensive fluorescence based technique for high-throughput antimalarial screening. Antimicrob Agents Chemother 48:1803–1806

47. Cantrell CL, Franzblau SG, Fischer NH (2001) Antimycobacterial plant terpenoids. Planta Med 67:685–694

48. Gu JQ, Wang Y, Franzblau SG, Montenegro G, Yang D, Timmermann BN (2004) Antitubercular constituents of *Valeriana laxiflora*. Planta Med 70:509–514

49. Mootz D (1965) The crystal structure of DL-allantoin. Acta Cryst 19:726–734

50. Asia NR, Fatma UA, Mayades S, Mutasem OT (2004) Investigation of the active constituents of *Portulaca oleraceae* (Portulacaceae) growing in Jordan. Pak J Pharm Sci 17:37–45

51. Pauli GF, Case RJ, Inui T, Wang Y, Cho S, Fischer NH, Franzblau SG (2005) New perspectives on natural products in TB drug research. Life Sci 78:485–494

52. Peterson LR, Shanholtzer CJ (1992) Tests for bactericidal effects of antimicrobial agents: technical performance and clinical relevance. Clin Microbiol Rev 5:420–432

53. Tiam ER, Bikobo SDN, Zintchem AAA, Nyemeck NM II, Ndedi EDFM, Diboué PHB et al (2019) Secondary metabolites from *Triclisia gilletii*(Menispermaceae) withantimycobacterial activity against *Mycobacterium tuberculosis*. Nat Prod Res 33:642–650

54. Trager W, Jensen JB (1976) Human malaria parasites in continuous culture. Science 193:673–675

55. Collins L, Franzblau SG (1997) Microplate alamar blue assay versus BACTEC 460 system for high-throughput screening of compounds against *Mycobacterium tuberculosis* and *Mycobacterium avium*. Antimicrob Agents Chemother 41:1004–1009

56. CLSI (2011) Susceptibility testing of Mycobacteria, Nocardiae, and other aerobic actinomycetes–second edition, Approved Standard M24–A2. Clinical and Laboratory Standards Institute, Wayne

57. Frisch MJ, Trucks GW, Schlegel HB, Scuseria GE, Robb MA, Cheeseman JR et al (2010) Gaussian 09, Revision B.01. Gaussian Inc., Wallingford

58. O'Boyle NM, Tenderholt AL, Langner KM (2008) J Comp Chem 29:839–845

59. Mirzaei M, Elmi F, Hadipour NL (2006) A systematic investigation of hydrogen-bonding effects on the ^{17}O, ^{14}N, and ^{2}H nuclear quadrupole resonance parameters of anhydrous and monohydrated cytosine crystalline structures: a density functional theory study. J Phys Chem B 110:10991–10996

60. Behzadi H, Hadipour NL, Mirzaei M (2007) A density functional study of ^{17}O, ^{14}N and ^{2}H electric field gradient tensors in the real crystalline structure of α-glycine. Biophys Chem 125:179–183

61. Coxon B, Fatiadi AJ, Sniegoski LT, Hertz HS, Schaffer R (1977) A novel acylative degradation of uric acid, Carbon-13 nuclear magnetic resonance studies of uric acid and its degradation products. J Org Chem 42:3132–3140

Publisher's Note